Recent Results on W − Physics from the UA2 Experiment at the CERN $p\bar{p}$ − collider

The UA2 Collaboration

Bern − Cambridge − CERN − Heidelberg − Milano −
Orsay (LAL) − Pavia − Perugia − Pisa − Saclay (CEN)

presented by
Karl Jakobs

CERN
Geneva, Switzerland

Abstract

The UA2 experiment at the CERN $p\bar{p}$ collider has collected large samples of W and Z events during the 1988 and 1989 data taking periods at $\sqrt{s}$ = 630 GeV. These data have been used to measure the production cross sections and the transverse momentum distributions of W and Z bosons and to compare them to QCD predictions. In the framework of the Standard Model, the ratio between the W and Z production cross section has been used to determine the total width of the W boson. A precise measurement of the ratio between the the W and Z masses has been extracted, leading to a new determination of the weak mixing angle $\sin^2\theta_w$. A combination of this result with recent measurements of the Z mass at e^+e^- colliders results in a precise absolute measurement of the W mass.

1. Introduction

The upgraded UA2 experiment at the CERN $p\bar{p}$ collider has collected data corresponding to an integrated luminosity of 7.4 pb^{-1} during the 1988 and 1989 running periods at peak luminosities of up to 3 x 10^{30} $cm^{-1}s^{-1}$. Large samples of $W \to e\nu$ and $Z \to e^+e^-$ events have been isolated from these data and have been used to measure the production and decay properties of the W and Z bosons.

In the present report the results of these measurements are presented and compared to the predictions of the Standard Model. After a brief description of the UA2 detector (section 2), the W and Z selection criteria are described (section 3). In section 4 the measured production cross sections times branching ratios are compared to QCD predictions, including partial corrections to second order in α_s. A more sensitive test of QCD is performed by comparing the measured transverse momentum distributions of the produced vector bosons to second order QCD predictions. In particular, the high P_T^W – region is examined for deviations from the theoretical predictions, which might indicate physics beyond the Standard Model. This analysis is presented in section 5.

Although recently our knowledge of the mass and width of the Z boson has been substantially improved from measurements at e^+e^- – colliders, it is still necessary to rely on hadron colliders for measurements of the mass and width of the W boson. The analysis of the UA2 data with the aim to obtain a precise measurement of the ratio of the W and Z masses is presented in section 6. This mass ratio has been combined with e^+e^- results for the Z mass leading to a precise absolute measurement of the W mass.

In addition, the data have been used to search for additional heavy vector bosons W′ and Z′, which arise in extensions of the minimal Standard Model. Mass limits for the production of such heavy bosons have been deduced and are presented in section 7.

2. The UA2 Detector

The UA2 detector was substantially upgraded between 1985 and 1987 [1]. A summary of parts relevant to the study of W and Z bosons is contained in Ref. [2], and only the major points are repeated here. Additional details about specific detector elements can be found in the references given below.

A quadrant of the detector is shown in Figure 1. The pseudorapidity (η) coverage of the central calorimeter [3] of $-1 < \eta < 1$ has been extended with new end cap calorimeters to $-3 < \eta < 3$ [4]. The same technique (lead and iron absorber plates with scintillator and wavelength shifter readout) is used throughout. An electromagnetic compartement with lead absorber plates of 17.0 – 24.4 radiation lengths (depending on the polar angle) is followed by hadronic compartements with iron absorber plates. In the central calorimeter, the hadronic region is subdivided in depth into two compartements of two interaction lengths each. The lateral segmentation in the central calorimeter is constant in azimuth and polar angle

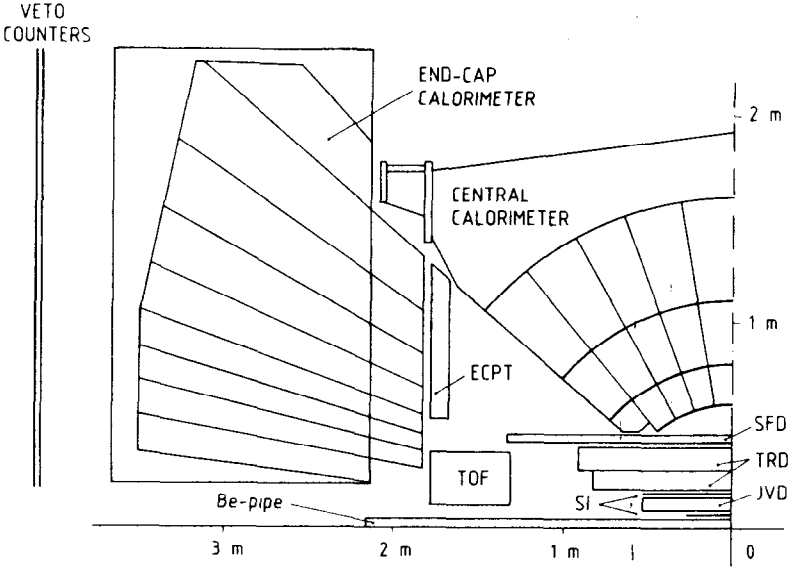

Figure 1: A schematic view of one quadrant of the UA2 detector.

($\Delta\phi = 15°, \Delta\theta = 10°$). In the end caps, the two cells closest to the beam axis ($2.5 < |\eta| < 3.0$ and $2.2 < |\eta| < 2.5$) cover 30° in azimuth, and the other cells have a constant segmentation $\Delta\phi = 15°, \Delta\eta = 0.2$.

The calorimeter response has been extensively studied in test beams of muons, pions and electrons during the period of 1986 and 1989. Initially all calorimeter cells were placed in the test beam to provide an absolute calibration. This energy scale has then been tracked using periodic ^{60}Co source and pulser calibrations. Each year, a portion of the calorimeter has been recalibrated in the test beam to verify this procedure, leading to an estimated error of 1% on the energy scale for the electromagnetic calorimetry.

Energy clusters are reconstructed in the calorimeter by joining all cells with an energy greater than 400 MeV sharing a common edge. Those clusters with a small lateral size and a small energy leakage into the hadronic compartements are marked as electromagnetic clusters and are subsequently examined as potential electron candidates.

The layout of the central detector is included in Figure 1. Around the beam pipe, at radii of 3.5 and 14.5 cm, are two arrays of silicon counters used for tracking and ionization measurements [5]. A cylindrical drift chamber (Jet Vertex Detector or JVD) [6] is located between the two layers of silicon. Its purpose is to confirm with a good resolution in ϕ the presence of a track close to the interaction point. Outside of these tracking detectors is a Transition Radiation Detector (TRD) [7], consisting of two sets of radiators and proportional chambers. Its purpose is to provide additional power to the electron identification. The outermost of the central detectors is the Scintillating Fibre Detector (SFD) [8], which consists of approximately 60000 fibres arranged on cylinders into 8 stereo triplets. Charged tracks and the position of the event vertex along the beam axis are reconstructed using the SFD in conjunction with the silicon hodoscopes and the JVD.

The last element before the calorimeters are the preshower detectors used to localize the early development of an electromagnetic shower initiated in a lead converter. In front of the central calorimeter, this function is served by the SFD, where 1.5 radiation length of lead are positioned before the last two stereo triplets of fibres. For the end cap region, the preshower detection is accomplished by the End Cap Proportional Tubes (ECPT) [9], which consist of a stereo triplet of proportional tubes behind a 2 radiation length lead converter. Two stereo triplets in front of the converter act as tracking chambers. In each case, an electron is identified by a large cluster of charge in the preshower region which lies close to the reconstructed track [2].

3. Selection of W and Z Events

3.1 W Selection

In the three level trigger system [10] of the UA2 experiment events are selected which have an electromagnetic cluster (small lateral size, small hadronic leakage) with a transverse energy greater than 12.0 GeV in the calorimeter. These events are searched for electron candidates by applying the standard UA2 electron identification [2], for which the following conditions have to be fulfilled:

- existence of a reconstructed track originating from the reconstructed event vertex and pointing to the electromagnetic calorimeter cluster;
- existence of a preshower cluster which is consistent with the position of the electron candidate track;
- the lateral and longitudinal profile of the energy shower in the calorimeter is required to be consistent with that expected from an electron incident along the observed track.

The presence of the neutrino in $W \rightarrow e\nu$ decays is deduced by measuring the electron energy and the energies of all particles (generally hadrons) recoiling against the W. The missing transverse momentum (P_T^{miss}) is attributed to the undetected neutrino:

$$\vec{P}_T^{\nu} \approx \vec{P}_T^{miss} = -(\vec{P}_T^{e} + \vec{P}_T^{had})$$

where $\vec{P}_T^{e}$ is the electron transverse momentum and $\vec{P}_T^{had}$ is the total transverse momentum of the recoiling hadrons. In order to extract a clean sample of $W \rightarrow e\nu$ events, the following kinematical cuts are applied in addition:

- $P_T^{e} > 20.0\ GeV, \qquad P_T^{\nu} > 20.0\ GeV$
- $M_T > 40.0\ GeV.$

M_T is the transverse mass of the electron−neutrino system, defined as $M_T = \sqrt{2 P_T^{e} P_T^{\nu} (1 - \cos\Delta\phi)}$, where $\Delta\phi$ is the azimuthal separation between the measured electron and neutrino directions.

These selection criteria result in a W sample of 1676 events with an electron in the central calorimeter, and 365 events with a forward electron. The samples are expected to contain a contribution of 3.8% and 3.3%, respectively, from the process $W \rightarrow \tau\nu$ followed by the decay $\tau \rightarrow e\nu\bar{\nu}$. The background from misidentified jets from QCD jet production is estimated to be less than 1%.

3.2 *Z Selection*

At the trigger level events with two electromagnetic clusters with transverse energies above 5.0 GeV and an azimuthal separation of more than 60° are selected. At least one of the two electron candidates must satisfy the standard electron identification, while the other one is allowed to satisfy looser cuts on the track preshower match (see Ref. [2] for details). This selection results in a total sample of 232 events with an invariant mass of the electron pair above 40 GeV. There are 54 events in the mass interval 40 − 70 GeV, which is in good agreement with the expected 24 ± 2 Drell − Yan events plus 32 ± 5 QCD background events. In the mass region 76 $< m_{ee} <$ 110 GeV, which is defined as the Z signal region, 169 events with an expected QCD background of 2.4 ± 0.3 events are found. One event is observed with m_{ee} = 278 GeV. The expected number of Drell − Yan pairs with masses greater than 160 GeV is 0.3 events.

4. W and Z Cross Sections

4.1 *Cross Section Measurement*

The cross section for W production is determined from the equation

$$\sigma_W^e = \frac{N_W - N_\tau}{\varepsilon \eta L}$$

where N_W is the observed number of W candidates, N_τ is the contribution from $W \to \tau \nu$ followed by the decay $\tau \to e \nu \bar{\nu}$, η is the acceptance of the geometrical and kinematic selections, ε is the overall electron efficiency, and L is the integrated luminosity. The acceptance η was calculated using a Monte Carlo program which generated W and Z boson production according to the transverse momentum and rapidity distributions of Ref. [11]. The Monte Carlo accounted for the effects of the event vertex distribution and for the precise geometry of the tracking, preshower and calorimeter detectors. The uncertainties on the acceptance were estimated by varying the structure functions and the transverse momentum distributions. The acceptance was found to be 53.0 ± 1.7 % for the central calorimeter region and 8.9 ± 0.8 % for the end cap region. The electron efficiency ε differs among the different calorimeter regions. It includes contributions from the vertex finding, trigger and preshower matching efficiencies, as well as from the overall calorimeter efficiency. Detailed numbers for the various efficiencies in the different calorimeter regions can be found in Ref. [2]. The combined electron efficiency, weighted by the acceptance of the different calorimeter regions, is found to be 64.8 ± 1.1 %. By using these numbers one obtains for the W cross section:

$$\sigma_W^e = 660 \pm 15\,(stat) \pm 37\,(syst) \quad pb.$$

To extract the production cross section of the Z boson, the following equation is used:

$$\sigma_Z^e = (N_Z - N_{QCD}) \frac{1 - f_\gamma}{\varepsilon \eta L}$$

where N_Z is the number of Z candidates, N_{QCD} is the number of background events from QCD jet production, f_γ is the relative contribution from single photon exchange and γZ interference terms. This contribution has been estimated to be 1.65 % in the mass region 76 $< m_{ee} <$ 110 GeV. The acceptance η was estimated by the same Monte Carlo simulation as in the case of the W and was found to be 49.6 ± 1.0 %. The combined electron efficiency ε, weighted over the various calorimeter regions, is found to be 63.3 ± 1.5 %. From these numbers and the observed event rates one obtains for the Z cross section:

$$\sigma_Z^e = 70.4 \pm 5.5\,(stat) \pm 4.0\,(syst) \quad pb.$$

The measured cross section values can be compared with the Standard Model predictions. In order to perform these comparisons, the following ingredients have been used:

- calculations of the branching ratios for the decays $W \to e \nu$ and $Z \to e e$ by taking into account all decay modes expected in the Standard Model. For quarks in the final states QCD corrections have been applied, including the effect of non − zero masses for the t and b quarks.
- the total W and Z cross section calculated at three different perturbative orders: (i) Born level, (ii) including the $O(\alpha_s)$ QCD corrections [11] and (iii) including a partial calculation of the $O(\alpha_s^2)$ corrections [12].

The theoretical predictions depend on a number of basic parameters. The value of α_s was computed using Λ_{QCD} as given from the structure function parametrization used and a scale $Q = M_W$. For the gauge boson masses the average values from SLC [13] and LEP [14] and the UA2 value of M_W / M_Z were used (see section 6). A serious uncertainty arises from the parton distribution functions. The standard set used was DFLM [15] with Λ_{QCD} = 0.160 GeV which has been evaluated using next − to − leading order QCD calculations and the DIS regularisation scheme. Two alternative sets, MRSE′ and MRSB′ [16] obtained from next − to − leading order QCD calculations performed in the $\overline{MS}$ scheme were also used.

The comparison of the measured cross sections to the Standard Model prediction as a function of the top mass is shown in Figure 2. The dependence of the predictions on m_{top} arises from the change in the total width of the W (Z) as the $W \to t\bar{b}$ ($Z \to t\bar{t}$) decay channels become kinematically suppressed. The $O(\alpha_s)$ correction to the total cross section amounts to an increase of 30% and the partial calculations of $O(\alpha_s^2)$ corrections indicate an additional increase in the cross section by 10%.

The experimental measurements agree well with the QCD predictions including the second order corrections for the assumption of a heavy top quark. However, due to the large theoretical and experimental uncertainties no quantitative conclusion on the mass of the top quark can be made. Figure 2 illustrates that the major theoretical uncertainty is coming from the parton distribution functions and is found to be comparable with the experimental uncertainty.

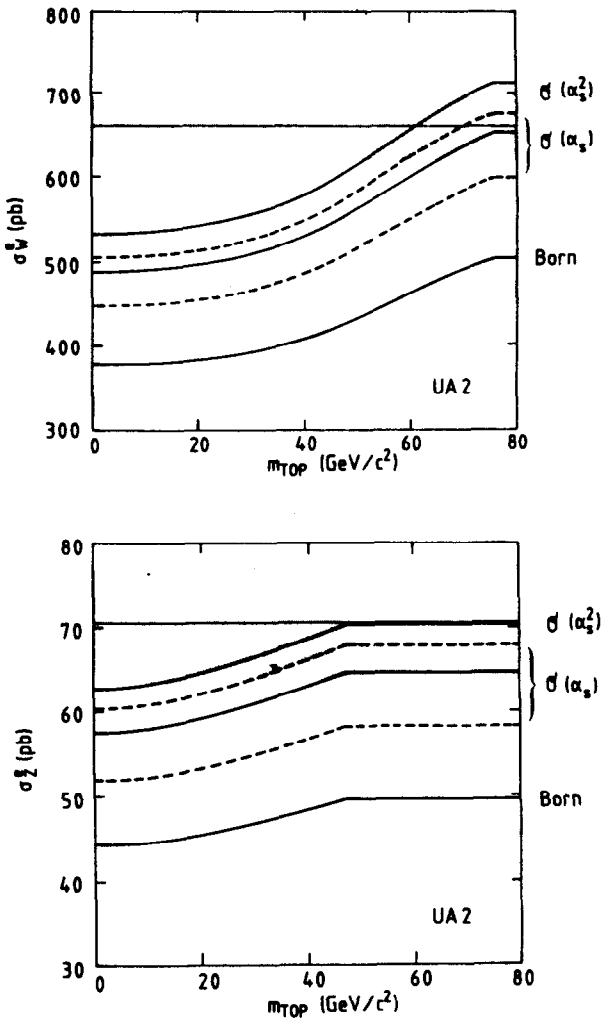

Figure 2. Comparison of the measured cross sections σ_W^* and σ_Z^* with Standard Model predictions as a function of m_{top}. The shaded band represents the 1 σ confidence interval, combining statistical and systematic errors in quadrature. The three solid curves indicate the result of the cross section calculations, using the DFLM parton distribution functions. The upper dashed curve uses the MRSB′ parametrizations, while the lower dashed curve uses the MRSE′ parametrizations.

4.2 Measurement of the W Width

Many systematic uncertainties, both experimental and theoretical, which contribute to the individual cross sections σ_W^* and σ_Z^* are common and cancel in the cross section ratio $R = \sigma_W^*/\sigma_Z^*$. Via the formula

$$R = \frac{\sigma_W^*}{\sigma_Z^*} = \frac{\sigma_W}{\sigma_Z} \frac{\Gamma(W \to e\nu)}{\Gamma_W} \frac{\Gamma_Z}{\Gamma(Z \to ee)}$$

this ratio is related to the total cross section for W (Z) production σ_W (σ_Z) and the total and partial widths for the boson decays.

In the past, this information has been used to place limits on the number of light neutrino generations [17]. Recent measurements by experiments at e^+e^- colliders [13,14] have now fixed the total Z width with relatively high precision, allowing R to be used to make a precise, albeit indirect, measurement of the total width of the W. This width is sensitive to the mass of the top quark m_{top} if $m_{top} + m_b < M_W$, where m_b is the mass of the b quark. From the equation above one obtains:

$$\Gamma_W = \frac{\sigma_W}{\sigma_Z} \frac{\Gamma(W \to e\nu)}{\Gamma(Z \to ee)} \frac{1}{R} \Gamma_Z$$

where the first two factors on the right hand side do not depend on the value assumed for the top quark mass. The uncertainties on the first two factors have been investigated by varying the parton distribution functions and changing the value of $\sin^2\theta_W$ from the value determined by UA2 (section 7) to the world average value determined from low energy neutrino experiments [18] while keeping M_Z fixed. For the width of the Z boson the weighted average of SLC [13] and LEP [14] is used, $\Gamma_Z = 2.546 \pm 0.032$ GeV. From the measured cross section values the value R is found to be

$$R = \frac{\sigma_W^*}{\sigma_Z^*} = 9.38^{+0.82}_{-0.72}(stat.) \pm 0.25(syst.)$$

which leads to the

$$\Gamma_W = 2.30 \pm 0.19(stat) \pm 0.06(syst) \quad GeV$$

where the errors reflect the experimental errors only. The theoretical uncertainties correspond to an uncertainty of less than 50 MeV on Γ_W. In the Standard Model the width of the W is expected to decrease from 2.8 GeV to 2.1 GeV as m_{top} is increased from zero to M_W. The measured value is in agreement with the Standard Model expectation in the case of a heavy top quark, and is inconsistent with a light top quark. At the 90 % confidence level Γ_W is found to be less than 2.56 GeV.

5. Transverse Momentum Distributions of W and Z

A study of the transverse momentum distributions of the W and Z bosons is of interest for several reasons. Firstly, the P_T dependence of the cross section provides a more sensitive test of QCD than the total cross section. In addition, one can look for deviations from the theoretical predictions which might indicate physics beyond the Standard Model. This is especially true for large P_T values, where the events are characterized by jets plus leptons and/or missing transverse energy. These are typical signatures in the searches for new physics processes such as heavy quark production or supersymmetry. Finally, good understanding of the P_T^W measurement is essential for a precise measurement of the W mass.

At low P_T values where multiple soft gluon emission is expected to dominate the initial state radiation, the production cross section is calculated using soft gluon resummation techniques [11]. In the high P_T regime ($P_T > 20$ GeV), the cross section is expected to be well described by QCD perturbation theory, and complete $O(\alpha_s^2)$ calculations are now available for this case [19].

5.1 Transverse Momentum of the Z − Boson

The transverse momentum of the Z boson P_T^Z is evaluated from the measured total transverse momentum of the two decay electrons. The P_T^Z spectrum is shown in Figure 3(a). The measurement errors on P_T^Z are dominated by the energy resolution of the calorimeter, and are estimated to be about 2 GeV. A more precise measurement can be made for the η component of P_T^Z, where the η direction is defined as the inner bisector of the angle between the transverse directions of the two electrons. This component is relatively insensitive to fluctuations in the electron energy measurement, relying mainly on the angles of the electrons which are well measured. A resolution of about 0.3 GeV is estimated. The distribution of P_η^Z is shown in Figure 3(b).

In Figure 3, the predictions of Ref. [11] are superimposed on the data. The curves have been modified to account for detector acceptance and resolution, and the predictions are normalized to the observed number of events. The principal theoretical uncertainties are due to the lack of precise knowledge of certain input parameters, namely Λ_{QCD}, the parton distribution functions, and the scale of the running coupling constant. A plausible range of variations is represented by changing the structure function parametrizations and accordingly the value of Λ_{QCD}. Curves are shown for Λ_{QCD} = 0.160, 0.260, 0.360 GeV (four − flavour values) where the appropriate DFLM structure functions are used in each case. Within the experimental and theoretical uncertainties there is good agreement between the data and the QCD prediction.

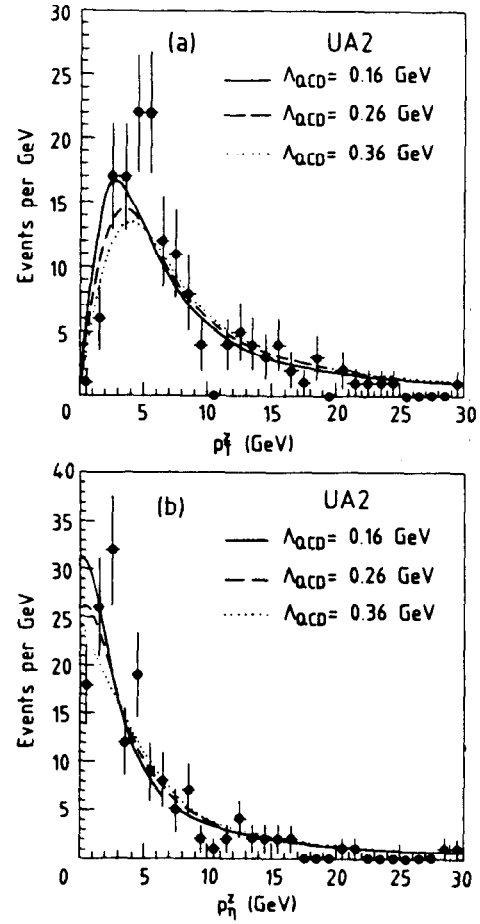

Figure 3. (a) The observed P_T^Z spectrum (points) compared with the QCD predictions of [11] for three different values of Λ_{QCD}. (b) The same comparison for the η component (see text) of P_T^Z.

5.2 *Transverse Momentum of the W – Boson*

The measurement of the transverse momentum of the W boson is more complex, since for its measurement the transverse momentum of the neutrino has to be used. As discussed in section 3 this requires the measurement of the transverse momentum of the system of hadrons recoiling against the W:

$$\vec{P}_T^{\,W} = \vec{P}_T^{\,e} + \vec{P}_T^{\,\nu} = -\vec{P}_T^{\,had} \quad .$$

Before comparing theoretical predictions with the data, detector effects have to be taken into account. Therefore one has to understand the resolution of the P_T^W measurement as well as any effects that might bias the P_T^W measurement by considering the system of recoiling hadrons. Such a bias can result from acceptance losses (hadrons escaping detection at small polar angles), calorimeter non – linearities and readout thresholds and also from the fact that for slow particles the energy measured by the calorimeter may be smaller than their momenta. Such effects can be investigated by studying the momentum balance between the electrons and the recoiling hadrons in $Z \rightarrow e^+e^-$ events. The momentum balance along the η direction $(P_\eta^Z(e^+e^-) - P_\eta^Z(had))$ is shown in Figure 4. The superimposed curve corresponds to the prediction of the detector response model. Since this model correctly reproduces the resolution and the small systematic shift, it can be used to correct the theoretical P_T^W distributions for detector effects.

Figure 5 shows the low momentum range of the P_T^W distribution compared to the calculations of [11] (curves). The consequences of uncertainties in the detector response are displayed in Figure 5(a). Figure 5(b) shows the same data compared to theory for different structure function parametrizations using different values for Λ_{QCD}. The agreement is quite good, but the uncertainty in the detector response precludes any quantitative conclusions.

For the high P_T^W tail of the distribution, the uncertainties in detector response are less important. In addition, in this region perturbative calculations are expected to be reliable and the data can be compared with the $O(\alpha_s^2)$ calculation of [19]. This comparison is shown in Figure 6, where the fraction of events is shown for $P_T^W > 20$ GeV. The theoretical prediction, obtained by using the DFLM structure function parametrization with $\Lambda_{QCD} = 0.160$ GeV is superimposed on the data. As for the low P_T^W region, there is good agreement between the data and the QCD prediction. In particular, there is no evidence for an excess of events at high P_T^W. In the data a fraction of 3.8 ± 0.6 (stat) $^{+0.9}_{-1.3}$ (syst) % of events is found with P_T^W values above 25 GeV. The second order QCD calculation gives an estimate of 2.8 ± 0.3 % for this fraction for the DFLM structure functions, where the error reflects the uncertainties due to the different DFLM sets. For the MRSB′ parametrization, the second order QCD prediction yields a fraction of 3.3 %.

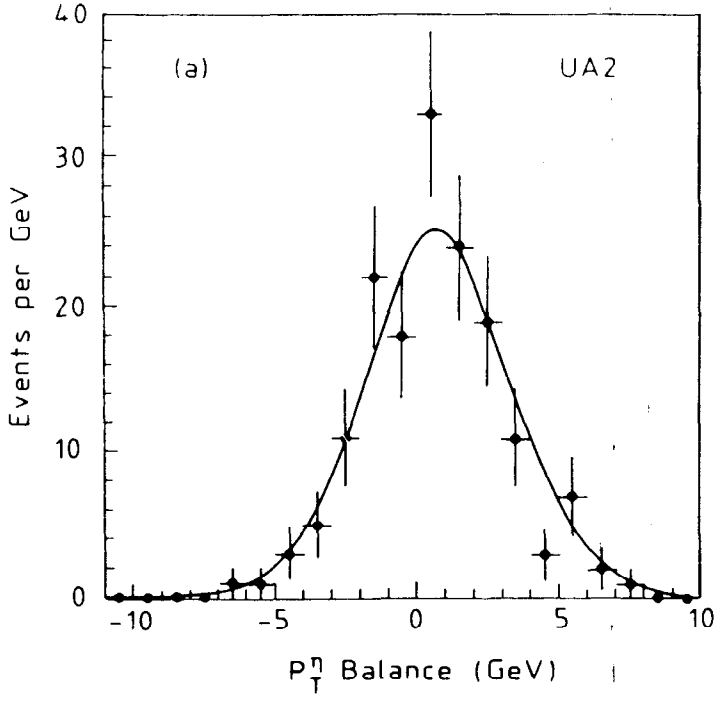

Figure 4. The momentum balance observed in $Z \rightarrow e^+e^-$ events along the η axis. The observed imbalance (points) is compared to the predictions of the detector response model (curve).

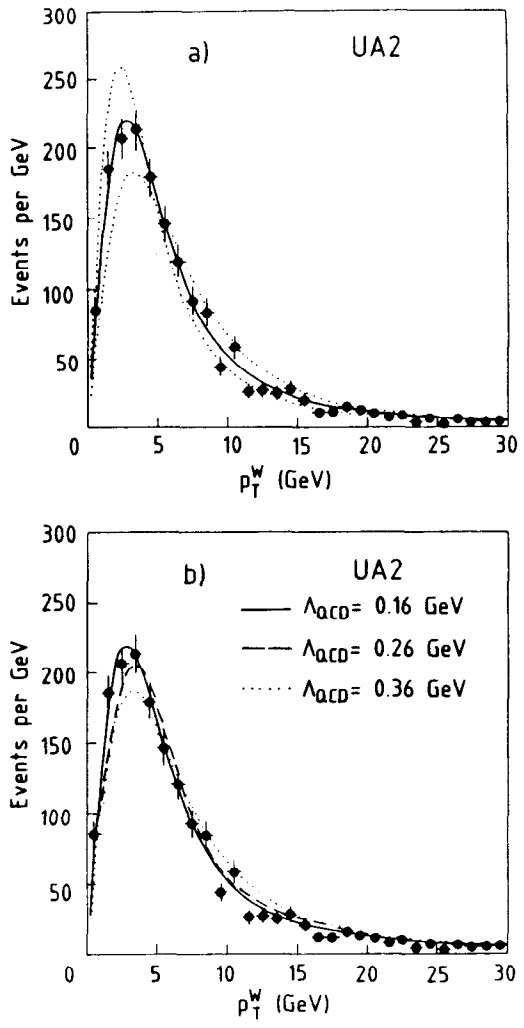

Figure 5. The observed P_T^W distribution (points) for $P_T^W < 30$ *GeV*. The curves show the QCD predictions of [11] (a) for Λ_{QCD} = 0.160 GeV using different models for the detector response, and (b) for three different values of Λ_{QCD}, using the best estimate for the detector response.

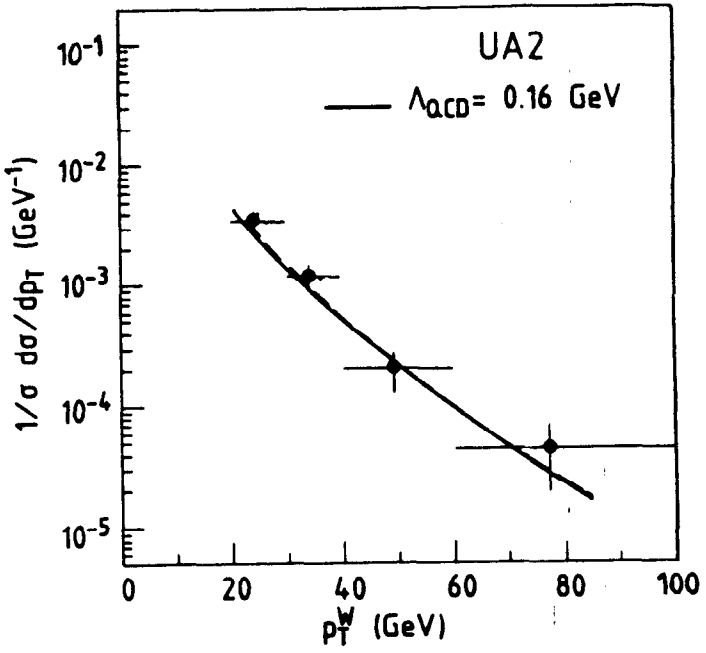

Figure 6. The observed fraction of high P_T^W events as a function of P_T^W. The curve represents the prediction of perturbative QCD [19] by using the DFLM structure function parametrization with Λ_{QCD} = 0.160 GeV.

6. Measurement of the W and Z Masses

Since the Z mass has been measured with high precision at e^+e^- colliders the ultimate goal is to measure the ratio M_W/M_Z with the smallest possible error at the hadron colliders and thereby to obtain a precise absolute measurement of the W mass. In order to guarantee a high quality of the energy reconstruction required for this purpose, additional fiducial cuts are applied to the data sample:

- W and Z candidates in which one or both of the electrons hit an edge cell ($0.8 \leq |\eta| \leq 1.0$) of the central calorimeter have been removed. These cells have significantly poorer energy resolution due to the modifications made to install the new central tracking detectors.[1]
- W and Z candidates in which one or both of the electrons hit a calorimeter cell close to a cell boundary have been removed. This cut eliminates 15 % of the total surface area of the central calorimeter.
- W candidates with P_T^W larger than 20 GeV have been removed.

Since the energy reconstruction systematics in the endcap and in the central calorimeter are different, the systematic errors on the electron energy measurement for electrons in different calorimeter regions are not identical. Furthermore the relative populations of W and Z events in the different calorimeter regions are different and the systematic errors will not cancel in taking the mass ratio. Therefore only those events in which the electron energy is measured in the fiducial volume of the central calorimeter are used for the mass analysis. These restrictions lead to samples of 1203 W events and 54 Z events with electrons in the central fiducial volume.

Because of the relatively small remaining Z sample we have defined an additional sample of Z events in which only one electron was required to be in the central fiducial region, whereas the other one was outside. These events have the energy of their second leg constrained by the requirement that the total momentum (electrons plus hadrons) is balanced in the transverse plane along a direction perpendicular to the bisector of the two electrons. The result is an independent sample of 94 Z events, which will be referred to as P_T−constrained sample in the following. The mass resolution for these events is worse, however their mass scale is derived from the energy calibration of the central fiducial region.

The masses of the W and Z bosons have been determined using a maximum likelihood fitting procedure. For the $Z \to e^+e^-$ decay, the extraction of the Z mass from the observed distribution of m_{ee} was relatively simple. It was possible to use an analytic likelihood function which is a good approximation to the expected line shape, followed by small corrections for the effects which were neglected in the simplified function.

For the $W \to e\nu$ decay, the lack of knowledge about the longitudinal momentum of the neutrino forces the use of transverse variables in the fitting procedure. Likelihood functions are obtained numerically for the transverse momenta P_T^e and P_T^ν, and the transverse mass M_T, using a detailed simulation of W production and decay, followed by a carefully tuned model of the detector response to the W decay products, implemented in the form of a Monte Carlo simulation which was optimized for the fitting problem.

The results of the fits for the Z mass are summarized in Table 1. The quoted errors are the statistical errors from the fit. In a first fit, the width of the Z is fixed to 2.5 GeV, as expected in the Standard Model when $Z \to t\bar{t}$ decays are kinematically forbidden. This fit is shown for the central sample in Figure 7(a), and for the P_T−constrained sample in Figure 7(b). In a second fit, the width is left free providing a test of the assumptions in the first fit.

Table 1: A summary of the fits to different Z samples.

Sample	Parameter	1 Parameter Fit	2 Parameter Fit
Central	m_Z (GeV)	91.69 ± 0.43	91.70 ± 0.45
(analytic meth.)	Γ_Z (GeV)	2.5	$2.96^{+0.98}_{-0.78}$
	Conf. Level	96%	99%
P_T(constrained)	m_Z (GeV)	91.51 ± 0.57	91.53 ± 0.59
(analytic meth.)	Γ_Z (GeV)	2.5	$2.94^{+1.16}_{-0.94}$
	Conf. Level	96%	97%
Central	m_Z (GeV)	91.71 ± 0.48	91.72 ± 0.50
(numeric meth.)	Γ_Z (GeV)	2.5	$3.06^{+0.98}_{-0.87}$
	Conf. Level	95%	84%

The mass of the W has been determined by using two different fits to the three kinematical variables. In the first the width of the W is fixed to 2.1 GeV, as expected in the Standard Model when $W \to t\bar{b}$ decays are kinematically forbidden. This fit is shown for the three kinematical variables in Figure 8. For the second fit, the width has been left free. The results of these fits are summarized in Table 2.

Table 2: A summary of the fits to different W distributions.

Sample	Parameter	1 Parameter Fit	2 Parameter Fit
Transverse Mass	m_W (GeV)	80.75 ± 0.31	80.78 ± 0.31
	Γ_W (GeV)	2.1	$1.89^{+0.47}_{-0.40}$
	Conf. Level	84%	89%
P_T(electron)	m_W (GeV)	80.79 ± 0.38	80.83 ± 0.39
	Γ_W (GeV)	2.1	$1.60^{+0.78}_{-0.68}$
	Conf. Level	95%	97%
P_T(neutrino)	m_W (GeV)	80.32 ± 0.41	80.33 ± 0.42
	Γ_W (GeV)	2.1	$2.03^{+0.82}_{-0.72}$
	Conf. Level	83%	88%

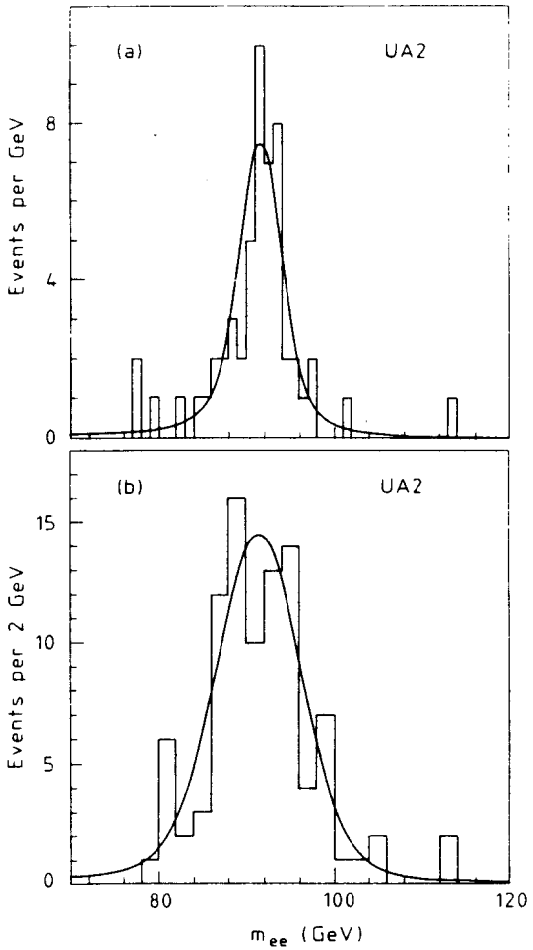

Figure 7. The fit to the invariant mass distribution for the Z sample with the fitted curves superimposed. (a) The central Z sample, (b) the P_T-constrained Z sample.

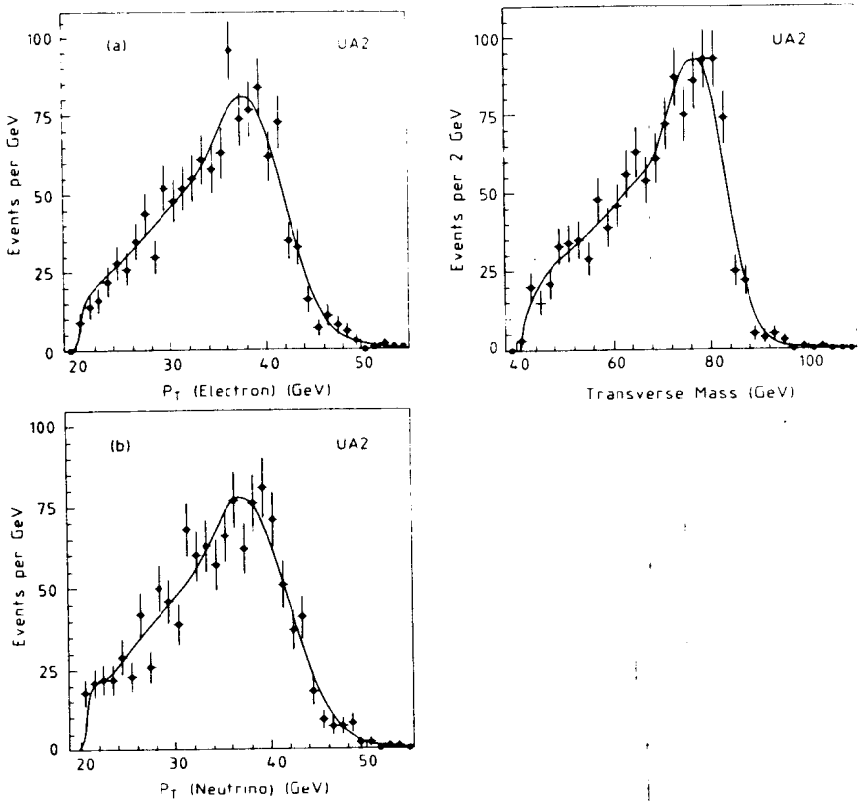

Figure 8. The fit to the transverse mass and transverse momentum distributions for the W sample with the fitted curves superimposed.

The most difficult aspect of the mass measurement involves the estimation of the systematic errors. For the Z, the following corrections and systematics were considered :

- variations in the underlying event contribution to the electron energy scale;
- the effect of radiative decays (i.e., unresolved γ from $Z \to e^+e^-\gamma$) ;
- variations in the parameters of the model for measuring P_T^{had} and their effect on the P_T – constrained fit.

These effects lead to an overall correction of -140 MeV, an overall systematic error of 120 MeV, and an additional systematic error of 100 MeV for the P_T – constrained fit. This additional systematic error for the P_T – constrained fit was added in quadrature to the corresponding statistical error. The final Z mass is computed by taking a weighted average of the two one-parameter analytic fits in Table 1. The result is :

$$M_Z = 91.49 \pm 0.35\,(stat) \pm 0.12\,(syst) \pm 0.92\,(scale)\ \ GeV,$$

where a scale error of 1.0% has be included, reflecting the systematic uncert nty in the energy calibration of the cent calorimeter fiducial volume.

For the W case, the analysis is more complex. The following list of effects has been considered:

- variations of the P_T^W distribution and variations in the model parameters for the measurement of P_T^{had};
- variations in the structure functions used in the Monte Carlo likelihood function;
- possible scale errors in the measurement of P_T^e;
- uncertainties in the electron resolution;
- variations in the underlying event contribution to the electron energy scale;
- variations in the Monte Carlo likelihood function attributed to the finite Monte Carlo statistics used;
- the effect of radiative decays (i.e.,unresolved γ from $W \to \gamma e\nu$).

These effects lead to an overall correction of $+40$ MeV, $+60$ MeV and $+160$ MeV, and an overall systematic error of 210 MeV, 300 MeV and 470 MeV for the M_T , P_T^e, and P_T^ν fits, respectively. The fit to the transverse mass gives the smallest errors, and is therefore quoted as the final value. The other two fits provide a significant cross – check of the method. The statistical errors for the fits are strongly correlated, but the results are quite consistent within the systematic erros alone. The final value for the W mass is then given by :

$$M_W = 80.79 \pm 0.31\,(stat) \pm 0.21\,(syst) \pm 0.81\,(scale)\ \ GeV,$$

where the 1% scale error has been included.

The two measurements of the boson masses can be combined to derive a value for M_W/M_Z. The energy scale contribution to the error on the ratio almost perfectly cancels. Thus the mass ratio is :

$$M_W/M_Z = 0.8831 \pm 0.0048\,(stat) \pm 0.0026\,(syst).$$

This result can be combined with recent results from SLC [13] and LEP [14] for the Z mass (a weighted average of $M_Z = 91.150 \pm 0.032$ GeV, including the current 30 MeV uncertainty in the LEP energy scale, was used) to give a rescaled W mass:

$$M_W = 80.49 \pm 0.43\,(stat) \pm 0.24\,(syst)\ \ GeV,$$

which can be compared with the value expected from the Standard Model.

In the Standard Model of the electroweak interactions, with a minimal Higgs sector, there are three fundamental free parameters (ignoring the Higgs and fermion masses). A convenient choice for these parameters, which reflects the precision of current measurements, is :

$$\alpha,\ G_\mu,\ M_Z\ .$$

A renormalization scheme must be chosen for the computation of higher order corrections. In this analysis, the scheme of Sirlin [20] is used:

$$\sin^2\theta_W = 1 - \frac{M_W^2}{M_Z^2}$$

leading to standard relations among the fundamental parameters:

$$M_W^2 = \frac{A^2}{(1-\Delta r)\sin^2\theta_W} \qquad \text{and} \qquad M_Z^2 = \frac{A^2}{(1-\Delta r)\sin^2\theta_W \cos^2\theta_W}$$

where

$$A = \sqrt{\frac{\pi\,\alpha}{\sqrt{2}\,G_\mu}} = 37.2805 \pm 0.0003\ \ GeV,$$

can be computed from current measurements of α and G_μ [21]. The variable Δr represents the radiative corrections arising from virtual loops in the boson propagators, and depends on the unknown masses m_{top} and m_{Higgs}. These corrections have been calculated within the context of the Minimal Standard Model, containing a single complex Higgs doublet.

Using the relations defined above, it is possible, given values for the Z mass and Δr, to predict a value for the W mass. This can be seen in Figure 9 where the dependence of Δr on m_{top} and m_{Higgs} is indicated by a series of lines in the (M_W, M_Z) plane. The UA2 result, in combination with that of SLC and LEP, has been marked by a data point whose errors reflect the combined statistical and systematic errors on the measurements. This data point lies within the region of the plane allowed by the Minimal Standard Model, and is consistent with a top quark which is heavier than the W.

Finally, the definition for the weak mixing angle given above can be used to convert the measurement of M_W/M_Z to a measurement of $\sin^2\theta_W$:

$$\sin^2\theta_W = 0.2202 \pm 0.0084\,(stat) \pm 0.0045\,(syst)$$

which is consistent with the world average value [18] derived from neutral current experiments:

$$\sin^2\theta_W = 0.2309 \pm 0.0029\,(stat) \pm 0.0049\,(syst).$$

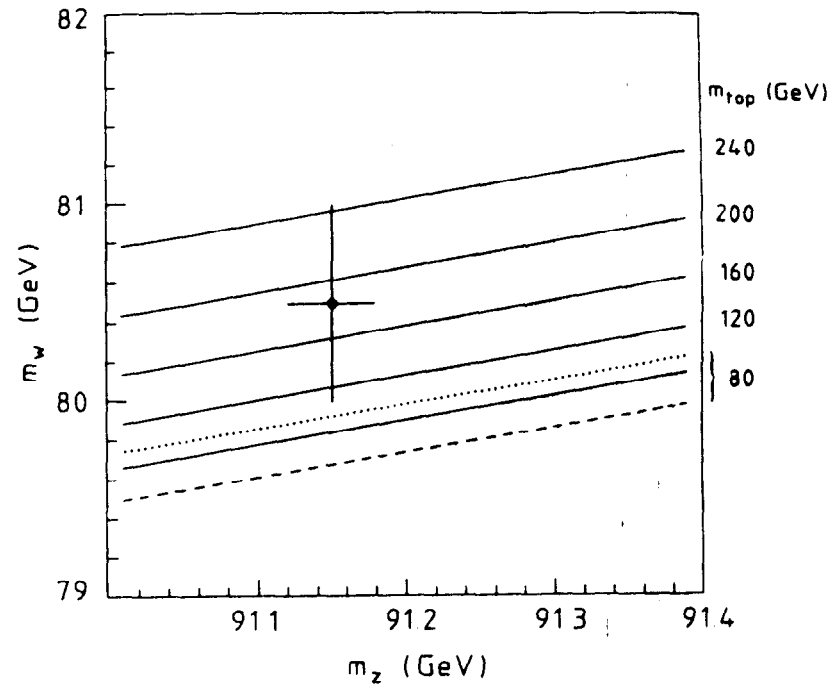

Figure 9. The comparison with the Minimal Standard Model predictions. The solid lines indicate the allowed values for M_W and M_Z for a given m_{top} with $m_{Higgs} = 100$ GeV. The dotted (dashed) line indicate the prediction for $m_{top} = 80$ GeV with $m_{Higgs} = 10$ (1000) GeV. The data point is defined in the text.

7. Search for Additional Vector Bosons

Additional vector bosons arise naturally in the framework of many possible extensions of the minimal SU(2) x U(1) Standard Model of electroweak interactions, whether it be through right-handed currents [22], composite models [23], or various models derived from superstring theories [24].

In the following, general limits on additional charged or neutral vector bosons are extracted, as a function of their mass, M_W (M_Z), their coupling to quarks λ_q, and their branching ratio to electrons, B_e, where λ_q and B_e are normalized to the Standard Model values. Using these variables, the cross section σ for the production of an additional vector boson and its subsequent decay is

$$\sigma = \sigma_0 \lambda_q^2 B_e$$

where σ_0 is the cross section for standard couplings. It is assumed, that

$$\Gamma_V = \Gamma_V \frac{M_V}{M_V} \qquad (V = W,Z)$$

where Γ_V and Γ_V are the total width of the additional and standard vector bosons, respectively.

In order to extract limits for W′ and Z′ production, their production and decay has been simulated using the DFLM structure function parametrization. A likelihood fit to the data sample using the transverse mass spectrum for the case of the W′ and the invariant mass spectrum of the two electrons for the case of the Z′ has been performed.

The results are shown in Figure 10(a) and (b) for the W′ and Z′ respectively as 95% confidence level contours in the (M_V , $\lambda_q^2 B_e$) plane. In the region of degenerate masses the observed rates for $W \to e\nu$ and $Z \to e^+e^-$ compared to the second order QCD prediction have been used to extract the confidence limits. In the high mass region, a W′ with $M_W <$ 247 GeV and a Z′ with $M_Z <$ 216 GeV can be excluded with 95% confidence, assuming Standard Model couplings.

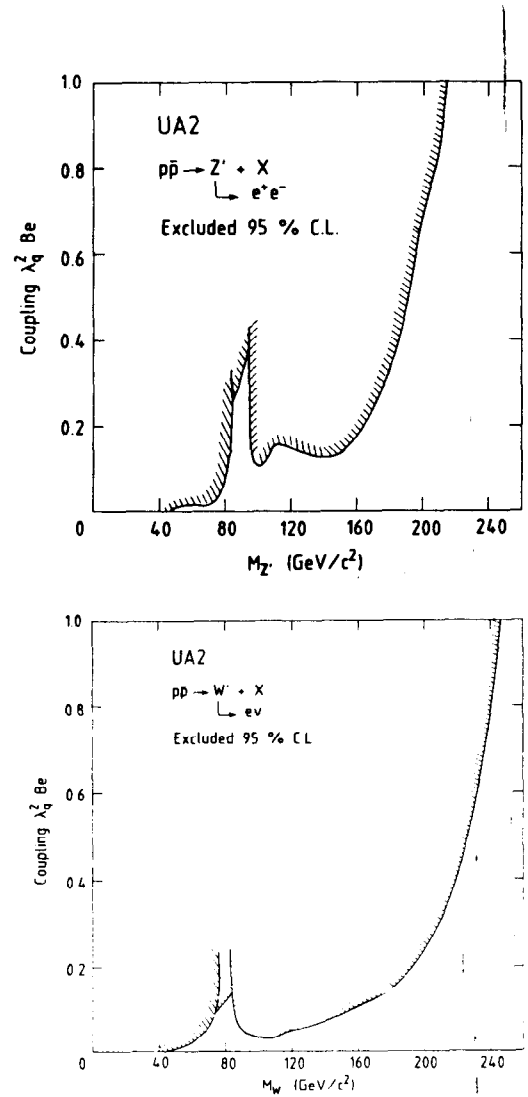

Figure 10. (a) Limits on an additional charged vector boson W′, shown as 95% confidence level contours in the (M_W , $\lambda_q^2 B_e$) plane, where λ_q, the W′ coupling to quarks, and B_e, the W′ branching ratio to electron-neutrino, are normalized to the Standard Model values.
(b) Same as (a) for an additional vector boson Z′ decaying into electron pairs.

8. Conclusions

The large W and Z data samples collected by the UA2 experiment have been used to extract improved measurements of the production and decay properties of W and Z bosons.

The production cross sections times branching ratio to electrons as well as the transverse momentum distributions are found to be in good agreement with QCD predictions. In particular the high P_T^W tail agrees with recent $O(\alpha_s^2)$ calculations, and shows no significant excess indicative of new physics processes.

From a precise measurement of the mass ratio M_W / M_Z a new value for the weak mixing angle $\sin^2\theta_W = 0.220 \pm 0.008$ (stat) $\pm$ 0.005 (syst), has been reported. From a combination of the measured mass ratio with recent measurements of the Z mass at SLC and LEP a precise absolute measurement of the W mass was obtained: $M_W = 80.49 \pm 0.43$ (stat) $\pm$ 0.24 (syst) GeV. The results of all measurements are in good agreement with the Minimal Standard Model and give support to the hypothesis that the top quark is heavier than the W.

The data have been used as well to set limits on the masses of possible additional charged (W′) or neutral (Z′) vector bosons. Assuming Standard Model couplings, a W′ with $M_{W'} < 247$ GeV and a Z′ with $M_{Z'} < 216$ GeV are excluded with a 95% confidence level.

9. References

[1] UA2 Collaboration, Proposal to improve the performance of the UA2 detector CERN/SPSC 84 – 30,84 – 95 and 85 – 3 (1984 and 1985, unpublished); UA2 Collaboration, C.N. Booth, Proc. 6th Topical Workshop on Proton Antiproton Collider Physics, Aachen 1986.

[2] UA2 Collaboration, J. Alitti et al., Z. Phys. C47 (1990) 11.

[3] A. Beer et al., Nucl. Instr. Meth. 224 (1984) 360.

[4] F. Alberio et al., The electron, jet and missing transverse energy calorimetry of the upgraded UA2 experiment at the CERN $p\bar{p}$ – ollider, in preparation for Nucl. Instr. Methods.

[5] R.Ansari et al., Nucl. Instr. Meth. A279 (1989) 388.

[6] F. Bosi et al., CERN – EP/89 – 82 (1989).

[7] R.Ansari et al., Nucl. Instr. Meth. A263 (1988) 51.

[8] R.E. Ansorge et al., Nucl. Instr. Meth. A265 (1988) 33; J. Alitti et al., Nucl. Instr. Meth. A279 (1989) 364.

[9] K.Borer et al., Nucl. Instr. Meth. A286 (1990) 128.

[10] G. Blaylock et al., The Multi – Level Trigger and Data Acquisition System of the Upgraded UA2 Experiment at the CERN $p\bar{p}$ – collider, in preparation for Nucl. Instr. and Meth.

[11] G. Altarelli et al., Nucl. Phys. B246 (1984) 12; G. Altarelli et al., Z. Phys. C27 (1985) 617.

[12] T. Matsuura, W.L. van Neerven, Z. Phys. C38 (1988) 623; T. Matsuura, S.C. van der Marck, W.L. van Neerven, Phys. Lett. B211 (1988) 171 and Nucl. Phys. B319 (1989) 570.

[13] MARK II Collaboration, G.S. Abrams et al., Phys. Rev. Lett. 63 (1989) 2173.

[14] ALEPH Collaboration, D. Decamp et al., Phys. Lett. B231 (1989) 519; DELPHI Collaboration, P. Aarnio et al., Phys. Lett. B231 (1989) 539; L3 Collaboration, B. Adeva et al., Phys. Lett. B231 (1989) 509; OPAL Collaboration, M.Z. Akrawy et al., Phys. Lett. B231 (1989) 530.

[15] M. Diemoz, F. Ferroni, E. Longo, G. Martinelli, Z. Phys. C39 (1988) 21.

[16] A.D. Martin, R.G. Roberts and W.J. Stirling, Mod. Phys. Lett. A4 (1989) 1135.

[17] UA2 Collaboration, R. Ansari et al., Phys. Lett. B186 (1987) 440; UA1 Collaboration, C. Albajar et al., Phys. Lett. B198 (1987) 271.

[18] G.L. Fogli, D. Haidt, Z. Phys. C40 (1988) 379.

[19] P.B. Arnold, M.H. Reno, Nucl. Phys. B319 (1989) 37.

[20] A. Sirlin, Phys. Rev. D22 (1980) 971.

[21] Particle Data Group: Review of Particle Properties, Phys. Lett. B204 (1988) 51.

[22] P. Langacker et al., Phys. Rev. D30 (1984) 1470.

[23] U. Baur et al., preprint MPI – PAE/PTH 29/85 (1985).

[24] E. Cohen et al., Phys. Lett. B165 (1985) 76;
F. del Aguila et al., Nucl. Phys. B287 (1987) 419;
D. London and J.L. Rosner, Phys. Rev. D34 (1986) 436.